DOI: 10.1002/ejic.201001135

Shape-Controlled Synthesis and Luminescent Properties of CeO_2:Sm^{3+} Nanophosphors

Yasutaka Yoshida[a] and Shinobu Fujihara*[a]

Keywords: Rare earths / Samarium / Cerium / Nanoparticles / Nanomaterials / Luminescence

CeO_2:Sm^{3+} nanophosphors were synthesized by hydrothermal treatments of aqueous solutions containing cerium nitrate, samarium nitrate, and sodium hydroxide. The shape of the nanocrystals was controlled simply by changing the hydrothermal treatment temperature. Nanorods of CeO_2:Sm^{3+} were obtained at 100 °C, whereas highly crystalline nanocubes were formed at a higher temperature of 180 °C. Photoluminescent properties of the nanophosphors were greatly influenced by their shapes. The as-prepared nanocubes exhibited much stronger orange-red emissions from Sm^{3+} than the as-prepared nanorods. A high-temperature treatment of the nanorods at 700 °C did not significantly enhance the emission intensity. The different photoluminescent properties were then examined by FTIR and Raman spectroscopy. Results showed that oxygen defects were the major reason for the inferior properties of the nanorods even after the high-temperature treatment. In contrast, the CeO_2:Sm^{3+} nanocubes were shown to be excellent nanophosphors prepared at 180 °C without any further treatment.

Introduction

Cerium dioxide (CeO_2), which has a cubic fluorite-type structure, is one of the most useful rare-earth oxides. Single-phase CeO_2 and its solid solutions with other lanthanide oxides (CeO_2–Ln_2O_3; Ln: lanthanide) or zirconium oxide (CeO_2–ZrO_2) have been recognized as important materials due to their excellent oxygen ion conductivity and oxygen storage capacity.[1,2] CeO_2 has found many industrial applications such as in solid oxide fuel cells,[3] automotive three-way catalyst systems,[4] and oxygen gas sensors.[5] Because of its band gap energy located at the near UV region, CeO_2 is also an excellent UV absorber.[6]

We have been focusing our attention on the luminescent properties of Ln^{3+}-doped CeO_2, which can be excited by near-UV light.[7–9] This is partially because recent advances in UV light-emitting diodes based on wide-gap semiconductors have facilitated solid-state white light using red, orange, yellow, green, and blue phosphors.[10] The shape of phosphors is controlled in accordance with their loading manner in practical devices. Nanometre-sized phosphor materials are attracting attention because of the prospect of specific applications such as electroluminescent devices, integrated optics, and biological labels.[11] Meanwhile the use of nanocrystalline or nanostructured CeO_2 has been expected to enhance its physicochemical performance due to its characteristic structural and electronic properties. For example, high porosity and high specific surface areas can increase active surfaces for catalysis and sensing. The electrical conductivity of CeO_2 nanoparticles is reportedly 10^4 times higher than the bulk material.[12] Elaboration of nanometre-sized CeO_2 with unique morphologies has been carried out to prepare nanocubes,[13] nanorods,[14] and nanowires[15] using organic templates. One-dimensional CeO_2 crystals are generally difficult to synthesize, and nanorods reported in the literature are often polycrystalline.

Recently, we have reported that CeO_2 nanorods can be hydrothermally synthesized starting from aqueous $CeCl_3$ solutions containing NaOH, polyethylene glycol (6000), and NaCl.[16] Observation by a high-resolution transmission electron microscopic (HRTEM) revealed that the nanorods were single crystals and their growth direction was along the [110] axis of the cubic CeO_2 structure. These results motivated us to study the synthesis and luminescent properties of highly crystalline CeO_2-based nanophosphors. In this work, CeO_2:Sm^{3+} nanorods and nanocubes were hydrothermally synthesized from aqueous $Ce(NO_3)_3$ and $Sm(NO_3)_3$ solutions containing a high concentration of NaOH without using organic templates. Morphological differences between the nanorods and nanocubes were controlled simply by changing the temperature of the hydrothermal treatment. The luminescence of Sm^{3+} was examined and is discussed in relation to the shape and defects of the CeO_2 nanocrystals.

Results and Discussion

White precipitates were obtained by hydrothermal treatment of basic Ce^{3+} and Sm^{3+} aqueous solutions at 100 and

[a] Department of Applied Chemistry, Keio University,
3-14-1 Hiyoshi, Kohoku-ku, Yokohama 223-8522, Japan
Fax: +81-45-566-1551
E-mail: shinobu@applc.keio.ac.jp

Supporting information for this article is available on the WWW under http://dx.doi.org/10.1002/ejic.201001135.

 © 2011 Wiley-VCH Verlag GmbH & Co. KGaA, Weinheim

180 °C. $[Sm^{3+}]/\{[Ce^{3+}]+[Sm^{3+}]\}$ ratios in the solutions were varied between 0 and 0.100 aiming for nominal $Ce_{1-x}Sm_xO_{2-y}$ (x = 0–0.100) compositions. Structural analysis was first carried out by X-ray diffraction (XRD). Figure 1 shows XRD patterns of the samples (x = 0, 0.001, 0.005, and 0.010) with the hydrothermal treatment temperature of 100 or 180 °C. All the patterns can be indexed with cubic fluorite-type structure (ICDD 34–394), indicating that the hydrothermal treatment is helpful for obtaining crystalline, single-phase CeO_2 samples for x = 0–0.010. When the Sm^{3+} content was increased to x = 0.100, additional peaks were detected in the XRD analysis due to the formation of a hexagonal $Sm(OH)_3$ phase in the sample heated at 100 °C. Sm^{3+} is reportedly hydrolyzed most easily among trivalent rare-earth ions as follows:[17]

$$Sm^{3+} + 3H_2O \rightleftarrows Sm(OH)_3 + 3H^+$$

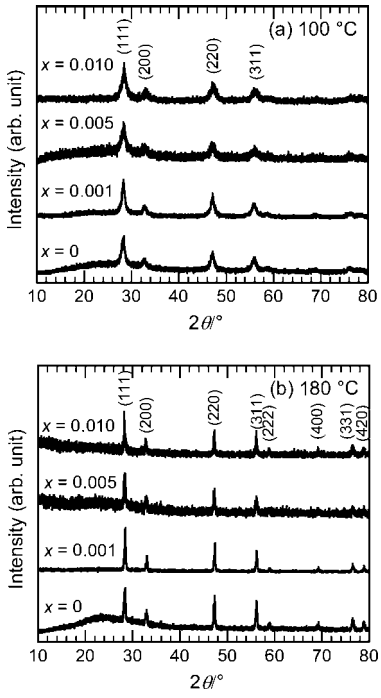

Figure 1. XRD patterns of the products obtained from the hydrothermal treatment of precursor solutions (x = 0, 0.001, 0.005, and 0.010) at (a) 100 and (b) 180 °C for 24 h.

At this point, it is not clear whether Sm^{3+} was doped in CeO_2 at the lower content range. This will be discussed later with results of photoluminescence (PL) measurements. For both the temperatures, the crystallinity of the samples appears to be slightly lowered with increasing the Sm^{3+} content from x = 0 to 0.010, judging from the peak broadening and the background noise. The effect of the hydrothermal treatment temperature is also seen from the patterns. The samples heated at 180 °C exhibit sharper diffraction peaks than those at 100 °C, which is attributed to the difference in the particle size and shape, as described below.

The morphology and shape of the CeO_2 samples were examined by field-emission scanning microscopy (FESEM) and HRTEM. Figure 2 shows FESEM and TEM images of the CeO_2 samples (x = 0–0.010) formed at 100 °C. In the FESEM images, a needle-like morphology is observed in the x = 0 sample. The particle size appears to be 200–500 nm in length. On increasing the Sm^{3+} content to x = 0.010, the aggregation of the particles seems to be promoted. In the TEM images, the shape of each particle is clearly defined as a nanorod. There is no clear difference in the size of the nanorods (20 nm in diameter and average 200 nm in length) in the samples between x = 0 and 0.010. Moreover, since the diameter of the nanorods is almost constant with respect to the length, the growth of a certain crystallographic plane seems to be substantially suppressed.

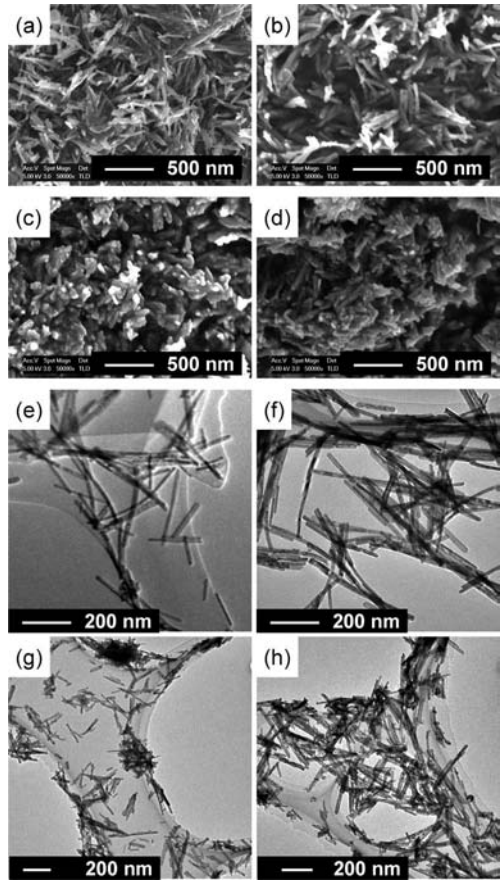

Figure 2. FESEM (a–d) and TEM (e–h) images of samples obtained by the hydrothermal treatment at 100 °C with Sm^{3+} content (a and e) x = 0, (b and f) x = 0.001, (c and g) x = 0.005, and (d and h) x = 0.010.

Figure 3 shows an HRTEM image of the nanorod from the x = 0 sample. The image highlights the structural uniformity of the nanorod with clearly resolved fringes of interplaner 0.31 nm spacings corresponding to the (111) plane of CeO_2. This (111) plane is at an angle of 55° with respect to the growing direction of the nanorod. The nanorod was then oriented along the [110] direction. From the viewpoint of thermodynamics, it is known that CeO_2 has three low-energy surfaces of (111), (110), and (310), and the (111) surface is the most stable.[18,19] Generally, a fast growing plane with higher surface energy tends to disappear leaving behind more slowly growing planes with lower surface energy. In this case, the low energy plane [possibly the (111)

 © 2011 Wiley-VCH Verlag GmbH & Co. KGaA, Weinheim

plane] covers the lateral surface of the nanorod. Usually one-dimensional CeO_2 particles are formed by using templates or surfactants to assist anisotropic crystal growth in solution synthesis.[20,21] In the absence of such the agents, the one-dimensional structure can be formed by an initial formation of hexagonal $Ce(OH)_3$ and subsequent transformation into CeO_2.[22] In our procedure, before heating, the solution was a purple-colored suspension after mixing of the starting rare-earth solution and the NaOH solution. This clearly indicates the formation of cerium hydroxide species which exhibit the ligand field effect on light absorption. The precipitates after the hydrothermal treatment were also purple, which changed to pale yellow on washing. This indicates the occurrence of Ce^{3+}/Ce^{4+} oxidation and CeO_2 formation in air.

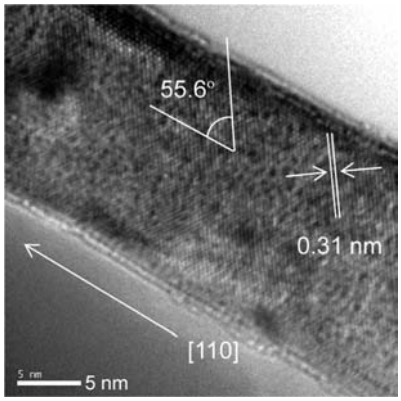

Figure 3. An HRTEM image of the nanorod sample (x = 0).

The morphology and shape of the CeO_2 samples (x = 0–0.010) formed at 180 °C are shown in Figure 4 in FESEM and TEM images. Cubic-faceted particles are clearly seen in the FESEM and TEM images at any Sm^{3+} content. At the higher temperature, the solubility of the $Ce(OH)_3$ species is enhanced in the aqueous solution. At the same time, Ce^{3+}/Ce^{4+} oxidation is promoted, thereby forming less soluble CeO_2. The direct formation of CeO_2 from solution reflects the crystallographic feature of the cubic fluorite-type structure, and then the cubic-shaped particles are grown. If any precipitates worked as a seed or templating crystal, the CeO_2 nanorods would be formed even at the higher hydrothermal treatment temperature.[23] Effects of intermediate hydrothermal treatment temperatures (120, 140, and 160 °C) on the morphological evolution of the nanorods and nanocubes were further examined by TEM (Supporting Information, Figure S1). Results demonstrated that small nanocubic crystallites were formed within the nanorods at 120 °C. The number of the nanocubes was then increased on increasing the temperature to 140 and 160 °C. Conversely, the nanorods decreased in number with the temperature. Thus, the increase in temperature promotes the decomposition or the dissolution of the $Ce(OH)_3$-derived nanorods and simultaneously the precipitation of the less soluble CeO_2 nanocubes.

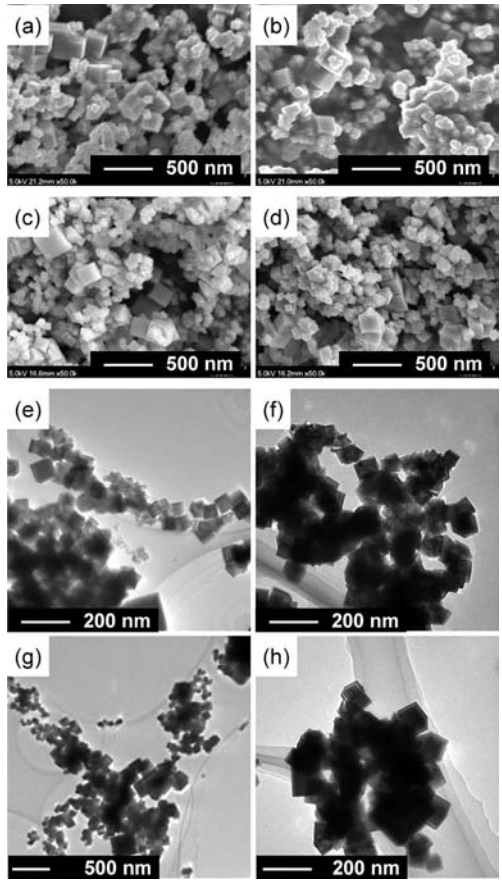

Figure 4. FESEM (a–d) and TEM (e–h) images of samples obtained by the hydrothermal treatment at 180 °C with Sm^{3+} content of (a and e) x = 0, (b and f) x = 0.001, (c and g) x = 0.005, and (d and h) x = 0.010.

An HRTEM image of the CeO_2 nanocube (x = 0) is shown in Figure 5. Clearly resolved fringes of interplaner 0.26 nm spacings correspond to the (200) plane of CeO_2. This (200) plane is parallel to the surface of the cube. The nanocube is then surrounded by the {100} plane. In terms of thermodynamics, however, the (100) plane is an energetically unfavorable surface due to the presence of dipole moments.[24] The unstable (100) surface of the nanocube is protected by certain chemical species during the crystal growth

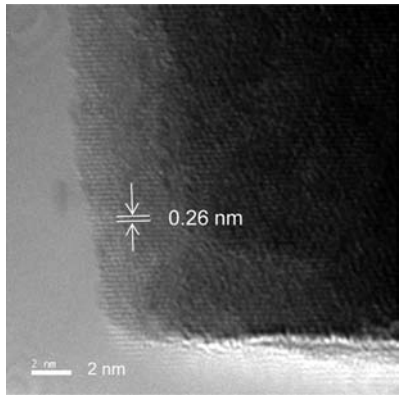

Figure 5. An HRTEM image of the nanocube sample (x = 0).

 © 2011 Wiley-VCH Verlag GmbH & Co. KGaA, Weinheim

in aqueous solution. This may be NO_3^- ions which are selectively adsorbed on the {100} plane.[25]

Optical properties of the CeO_2 nanorods and nanocubes were examined first with diffuse reflectance spectra, which can evaluate light scattering and absorption in powdered samples. Figure 6 shows diffuse reflectance spectra of the nanorods and nanocubes in the wavelength range 200–800 nm. In the visible region, the samples exhibit reflectance of 70–80%, which means that they do not absorb visible light. A slightly lower reflectance of the nanorods than the nanocubes comes from the transmission loss in the sparsely packed nanorods in the measurement. An abrupt decrease in reflectance at around 400 nm corresponds to the interband absorption of CeO_2 by the charge transfer from the O^{2-} valence band to the Ce^{4+} conduction band.

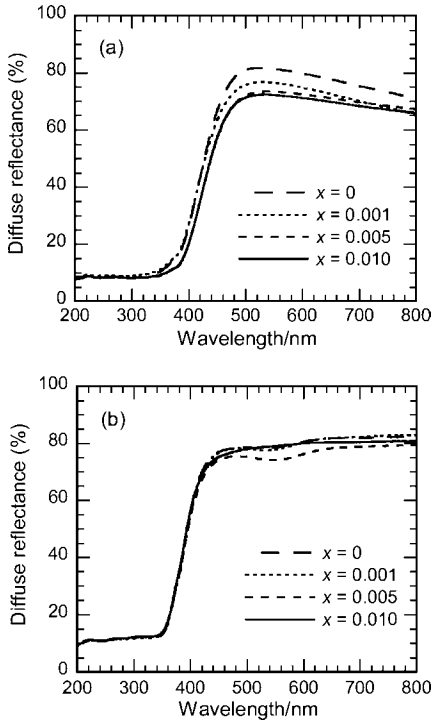

Figure 6. Diffuse reflectance spectra of (a) nanorods and (b) nanocubes with x = 0–0.010.

PL properties greatly depended on the shape of the nanocrystalline CeO_2 samples. Additionally, the size of the samples was also a concern. We paid attention to the size effect in terms of scattering of the emitted light taking into account the diffuse reflectance data shown in Figure 6. The nanocubes were found to exhibit much better PL properties than the nanorods in the as-prepared state. Figure 7 shows PL excitation ($\lambda_{em.}$ = 574 nm) and emission ($\lambda_{ex.}$ = 350 nm) spectra of the CeO_2:Sm^{3+} nanocubes (x = 0.001–0.010). It is seen that the PL intensity increases with increasing the Sm^{3+} content, indicative of the successful incorporation of Sm^{3+} into the CeO_2 lattice. A further increase in the Sm^{3+} content resulted in a decrease in the PL intensity due to concentration quenching. The PL excitation spectra show a broad excitation band with a peak around 350 nm. The band gap of CeO_2 is reported to be 3.4 eV (365 nm), suggesting that the excitation is achieved through the charge transfer between the O^{2-} valence band and the Ce^{4+} conduction band and the subsequent energy transfer to Sm^{3+}. The excitation efficiency shows its maximum near the absorption edge of CeO_2, indicating that the energy transfer process is promoted from electrons excited into the bottom of the Ce^{4+} conduction band. Electrons excited into higher energy levels in the conduction band may decay to the valence band nonresonantly with Sm^{3+}. The PL emission spectra of the CeO_2:Sm^{3+} nanocubes have two groups of emission lines which lead to orange-red colors. One is that of the $^4G_{5/2} \rightarrow {}^6H_{5/2}$ transitions (558, 561, and 574 nm) and the other is that of the $^4G_{5/2} \rightarrow {}^6H_{7/2}$ transitions (611, 614, and 619 nm). Both groups are allowed magnetic dipole transitions. According to the selection rule, magnetic dipole transitions that obey $\Delta J = 0$ and ± 1, where J is the total angular momentum, are allowed for Sm^{3+} in a site with inversion symmetry as in the case of the fluorite-type cubic CeO_2 crystal.

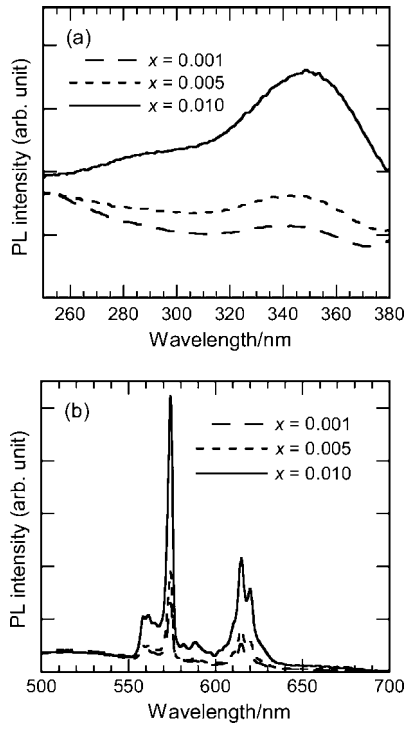

Figure 7. (a) PL excitation ($\lambda_{em.}$ = 574 nm) and (b) PL emission ($\lambda_{ex.}$ = 350 nm) spectra of nanocube samples with x = 0.001–0.010.

Because the PL intensity of the nanorod samples was relatively low, we tried to enhance the emission by a high-temperature treatment at 700 °C. This temperature was chosen because of the observation in our previous work that nanocrystalline CeO_2:Sm^{3+} films showed excellent PL properties after heating at 700 °C.[7] Figure 8 compares PL excitation ($\lambda_{em.}$ = 574 nm) and emission ($\lambda_{ex.}$ = 350 nm) spectra of the as-prepared nanocubes, the as-prepared nanorods, and the heat-treated nanorods with the x = 0.010 composition of CeO_2:Sm^{3+}. The high-temperature treatment does not have a significant effect on the PL properties of the nanorod samples. The PL intensity of the nanorods heated

 © 2011 Wiley-VCH Verlag GmbH & Co. KGaA, Weinheim

at 700 °C is still much lower than that of the nanocubes prepared at 180 °C. Therefore, it seems that the shape of the nanocrystals is greatly related to the PL properties of CeO_2:Sm^{3+}.

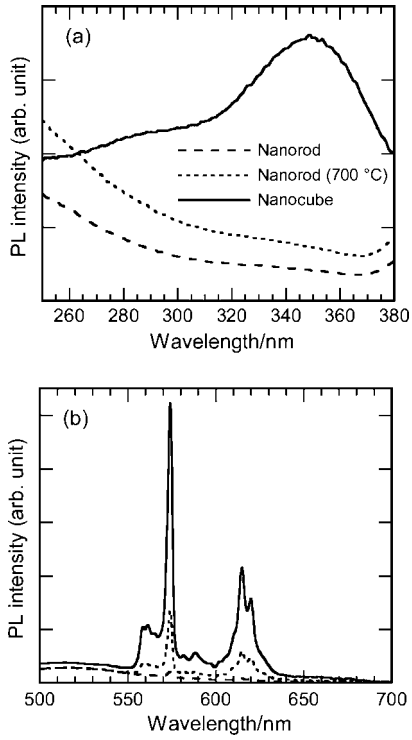

Figure 8. (a) PL excitation ($\lambda_{em.}$ = 574 nm) and (b) PL emission ($\lambda_{ex.}$ = 350 nm) spectra of the as-prepared nanorods, the as-prepared nanocubes, and the heat-treated nanorods with x = 0.010.

Structural analyses were performed further by FTIR and Raman spectroscopy to investigate the differences between the nanorods and nanocubes. Figure 9 compares FTIR and Raman spectra of the as-prepared nanocubes, the as-prepared nanorods, and the heat-treated nanorods. The as-prepared nanorods exhibit IR absorption bands at 3430, 1630, 1500, and 1370 cm^{-1}. The bands at 3430 and 1630 cm^{-1} are assigned to the stretching O–H and bending H–OH vibrations, respectively, thereby indicating the presence of water adsorbed on the nanorods or incorporated in the hydrated $CeO_2{\cdot}nH_2O$ crystal. The bands at 1500 and 1370 cm^{-1} are attributed to NO_3^- ions. The nanorods were washed six times with ion-exchanged water after the hydrothermal treatment. The presence of the NO_3^- ions implies their strong adsorption ability on the surface of the nanorods. After heating the nanorods at 700 °C, the IR absorption due to water and the nitrate ions is considerably lowered, which indicates that their removal from the nanorods is almost complete. The IR spectrum of the nanocubes coincides with that of the heat-treated nanorods. Therefore, the presence and absence of water and nitrate ions cannot explain the different PL properties of the nanorods and the nanocubes shown in Figure 8.

Raman spectra are used to discuss the structural defects. A Raman peak appearing at 450 cm^{-1} is caused by symmetric vibrations of the Ce–O8 unit and is an excellent indicator for lattice defects. The width and symmetry of this peak are sensitive to any disorder in the oxygen sublattice resulting from thermal and/or grain size-induced nonstoichiometry.[26] As shown in Figure 9, the Raman peak of the as-prepared nanorods is broader than that of the as-prepared nanocubes. This indicates that the nanorods have far more oxygen defects than the nanocubes. The high-temperature treatment of the nanorods has little effect on reducing the peak broadening. Therefore, the heat-treated nanorods still have more oxygen defects than the nanocubes. This explains the lower PL intensities of the as-prepared and the heat-treated nanorods than the as-prepared nanocubes. The PL properties of the nanocubes are almost unchanged even after heating them at 700 °C.

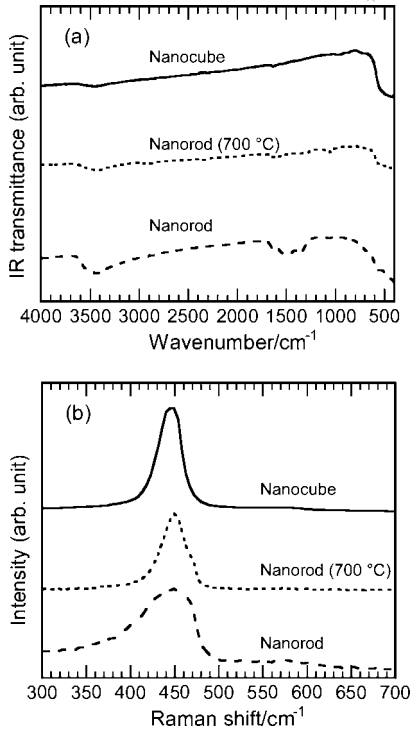

Figure 9. (a) FTIR and (b) Raman spectra of the as-prepared nanorods, the as-prepared nanocubes, and the heat-treated nanorods with x = 0.010.

To discuss the dependence of the PL intensity ($\lambda_{em.}$ = 574 nm) on the Sm^{3+} content, we initially examined thin-film samples prepared by a previously reported method.[7,8] The maximum PL intensity was observed at x = 0.001 (0.1%) (Figure S2). In the thin-film samples, the batch and the final Sm^{3+} content are almost the same and concentration quenching occurs beyond 0.1%. On the other hand, the nanocrystalline samples may have different Sm^{3+} contents compared with those of the batch aqueous solutions. This inference appears to be true; Figure 10 shows the maximum intensity observed at x = 0.010 (1.0%) and 0.005 (0.5%) for the nanocubes and the nanorods, respectively. Therefore the actual Sm^{3+} contents can be estimated to be approximately one tenth of the batch contents. Furthermore, the difference in the critical concentration for quenching between the nanocubes and the nanorods may result from the oxygen defects.

 © 2011 Wiley-VCH Verlag GmbH & Co. KGaA, Weinheim

The doping of the aliovalent Sm^{3+} ions in the CeO_2 lattice fundamentally induces the oxygen defects. The nanorod samples would be more severely influenced by the defects brought additionally by Sm^{3+}-doping, thus quenching the emissions at the lower doping level.

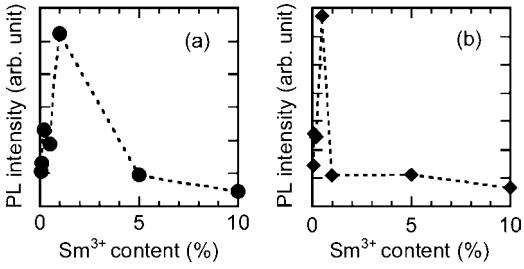

Figure 10. The dependence of the PL intensity at 574 nm on the Sm^{3+} content for (a) the as-prepared nanocubes and (b) the heat-treated nanorods.

Conclusions

CeO_2:Sm^{3+} nanophosphors with different shapes were synthesized by the hydrothermal treatment of the aqueous rear-earth solutions. The nanorods and the nanocubes were obtained by the hydrothermal treatment at 100 and 180 °C, respectively. The as-prepared nanorods showed inferior PL properties compared to those of the as-prepared nanocubes. Even after heating the nanorods at 700 °C, the PL properties were not enhanced. From the FTIR and Raman spectroscopic analysis, the nanorods were found to have far more oxygen defects than the as-prepared nanocubes. Our results demonstrate that the shape of the nanocrystals is of prime importance in designing and synthesizing nanophosphors because shape-related structural defects govern their luminescent properties.

Experimental Section

Sample Preparation: $Ce(NO_3)_3{\cdot}6H_2O$ and $Sm(NO_3)_3{\cdot}6H_2O$ (Wako Pure Chemical Industries Co., Ltd., Japan) were separately dissolved in ion-exchanged water. The resultant solutions were mixed and stirred for 10 min to obtain a solution containing Ce^{3+} and Sm^{3+} (5 mL). $[Sm^{3+}]/\{[Ce^{3+}] + [Sm^{3+}]\}$ ratios were varied between 0 and 0.100 aiming for nominal $Ce_{1-x}Sm_xO_{2-y}$ (x = 0–0.100) compositions. NaOH (22.4 g) was dissolved in ion-exchanged water (35 mL). The Ce^{3+}/Sm^{3+} solution (5 mL) was poured into the NaOH solution and stirred vigorously for 30 min, resulting in a precursor solution with the NaOH concentration of 14 mol/L.

The precursor solutions were placed in Teflon-lined autoclaves and heated at 100 or 180 °C for 24 h. Powder products in the solutions were washed with deionized water repeatedly and dried at 60 °C. The products obtained at 100 °C were heat-treated at 700 °C for 2 h.

Characterization: Crystalline phases of the samples were indentified with an X-ray diffractometer (Bruker AXS D8) using Cu-K_α radiation. The morphology of the samples was observed with FESEM (Hitachi S-4700). The particle shape was observed with HRTEM (Philips TECNAI F20). Diffuse reflectance spectra of the powder samples were recorded with a UV/Vis/NIR spectrophotometer (JASCO V-670) using an integrating sphere (ISN-723). Photoluminescence spectra were measured at room temperature with a spectrofluorophotometer (Shimadzu RF-5300PC) using a xenon lamp (150 W) as a light source. Careful attention was paid to avoid any misinterpretation of the spectra possibly coming from the apparatus and measurement conditions. Emission scans were performed with 1.5 nm band-pass emission slits. A filter was used to remove a second-order peak of the excitation light. The structure of the samples was also examined by FTIR spectroscopy (Bruker ALPHA) using a KBr disc. Raman spectra were measured using an Ar laser at 532 nm (CHROMEX Raman-One-CCD).

Supporting Information (see footnote on the first page of this article): TEM images for the samples hydrothermally treated at intermediate temperatures and the dependence of PL intensity on the Sm^{3+} content for the thin-film samples.

Acknowledgments

This work was supported by the Japan Society for the Promotion of Science (JSPS), Grant-in-Aid for Scientific Research (grant number 19560682). We thank Mr. M. Oikawa for his help with the preparation of the thin-film samples.

[1] M. Mogensen, N. M. Sammes, G. A. Tompsett, *Solid State Ionics* **2000**, *129*, 63–94.
[2] A. Suda, Y. Ukyo, H. Sobukawa, M. Sugiura, *J. Ceram. Soc. Jpn.* **2002**, *110*, 126–130.
[3] T. Mori, J. Drennan, J. H. Lee, J. G. Li, T. Ikegami, *Solid State Ionics* **2002**, *154–155*, 461–466.
[4] S. I. Matsumoto, *Catal. Today* **2004**, *90*, 183–190.
[5] N. Izu, W. Shin, N. Murayama, S. Kanzaki, *Sens. Actuators B* **2002**, *87*, 95–98.
[6] S. Tsunekawa, T. Fukuda, A. Kasuya, *J. Appl. Phys.* **2000**, *87*, 1318–1321.
[7] S. Fujihara, M. Oikawa, *J. Appl. Phys.* **2004**, *95*, 8002–8006.
[8] M. Oikawa, S. Fujihara, *J. Eur. Ceram. Soc.* **2005**, *25*, 2921–2924.
[9] M. Oikawa, S. Fujihara, *J. Solid State Chem.* **2005**, *178*, 2036–2041.
[10] U. Kaufmann, M. Kunzer, K. Kohler, H. Obloh, W. Pletschen, P. Schlotter, J. Wagner, A. Ellens, W. Rossner, M. Kobusch, *Phys. Status Solidi A* **2002**, *192*, 246–253.
[11] V. Buissette, D. Giaume, T. Gacoin, J. P. Boilot, *J. Mater. Chem.* **2006**, *16*, 529–539.
[12] Y. M. Chiang, E. B. Lavik, I. Kosacki, H. L. Tuller, J. Y. Ying, *Appl. Phys. Lett.* **1996**, *69*, 185–187.
[13] S. W. Yang, L. Gao, *J. Am. Chem. Soc.* **2006**, *128*, 9330–9331.
[14] C. Sun, H. Li, H. Zhang, Z. Wang, L. Chen, *Nanotechnology* **2005**, *16*, 1454–1463.
[15] C. W. Sun, H. Li, Z. X. Wang, L. Q. Chen, X. J. Huang, *Chem. Lett.* **2004**, *33*, 662–663.
[16] Y. Higashine, S. Fujihara, *J. Ceram. Soc. Jpn.* **2007**, *115*, 916–919.
[17] E. Bentouhami, G. M. Bouet, J. Meullemeestre, F. Vierling, M. A. Khan, *C. R. Chim.* **2004**, *7*, 537–545.
[18] T. X. T. Sayle, S. C. Parker, C. R. A. Catlow, *Surf. Sci.* **1994**, *316*, 329–336.
[19] J. C. Conesa, *Surf. Sci.* **1995**, *339*, 337–352.
[20] B. Tang, L. Zhuo, J. Ge, G. Wang, Z. Shi, J. Niu, *Chem. Commun.* **2005**, 3565–3567.
[21] D. Zhang, H. Fu, L. Shi, C. Pan, Q. Li, Y. Chu, W. Yu, *Inorg. Chem.* **2007**, *46*, 2446–2451.
[22] C.-C. Tang, Y. Bando, B.-D. Liu, D. Golberg, *Adv. Mater.* **2005**, *17*, 3005–3009.

 © 2011 Wiley-VCH Verlag GmbH & Co. KGaA, Weinheim

[23] P. X. Huang, F. Wu, B. L. Zhu, X. P. Gao, H. Y. Zhu, T. Y. Yan, W. P. Huang, S. H. Wu, D. Y. Song, *J. Phys. Chem. B* **2005**, *109*, 19169–19174.
[24] W. H. Lee, P. Shen, *J. Cryst. Growth* **1999**, *205*, 169–176.
[25] Q. Wu, F. Zhang, P. Xiao, H. Tao, X. Wang, Z. Hu, Y. Lü, *J. Phys. Chem. C* **2008**, *112*, 17076–17080.
[26] I. Kosacki, T. Suzuki, H. U. Anderson, P. Colomban, *Solid State Ionics* **2002**, *149*, 99–105.

Received: October 25, 2010
Published Online: February 23, 2011

 © 2011 Wiley-VCH Verlag GmbH & Co. KGaA, Weinheim